



Contents lists available at ScienceDirect

Arabian Journal of Chemistry

journal homepage: [www.ksu.edu.sa](http://www.ksu.edu.sa)

# Carbonized hemp hurd powder for eco-friendly polybenzoxazine composite brake material: Excellent friction property and high mechanical performance

Nuttarika Kunaroop<sup>a</sup>, Sarawut Rimdusit<sup>a</sup>, Phattarin Mora<sup>b</sup>, Salim Hiziroglu<sup>c</sup>,  
Chanchira Jubsilp<sup>b,\*</sup>

<sup>a</sup> Center of Excellence in Polymeric Materials for Medical Practice Devices, Department of Chemical Engineering, Faculty of Engineering, Chulalongkorn University, Bangkok, 10330, Thailand

<sup>b</sup> Department of Chemical Engineering, Faculty of Engineering, Srinakharinwirot University, Nakhonnayok 26120, Thailand

<sup>c</sup> Natural Resource Ecology and Management, Oklahoma State University, Stillwater, 74078, OK, U.S.A

## ARTICLE INFO

### Keywords:

Biocomposites  
Biochar  
Friction materials  
Industrial applications  
Circular economy

## ABSTRACT

Non-asbestos and non-copper polybenzoxazine friction composites were developed with varying mass ratios of synthetic graphite (SG)/carbonized hemp hurd (CHH). Mechanical, thermal, and tribological properties of the polybenzoxazine friction composites were studied. The wear simulation of the polybenzoxazine friction composites has been performed with commercial ANSYS finite element analysis software. The strength and modulus under flexure mode, glass transition temperature of the polybenzoxazine friction composite samples were observed to be improved with increasing CHH content. It appears that the incorporation of the CHH into the polybenzoxazine friction composites not only enhanced the coefficient of friction (COF) but also improved the overall wear resistance of the units. The wear resistance and wear pattern obtained by the wear simulation also showed a good correlation with the experimental results. Based on the findings in this study, it is evident that the carbonized hemp hurd possesses a great potential to be used in green brake pad application.

## 1. Introduction

There is a great interest to develop materials with enhanced friction and wear based on engineering polymer serving industries for a variety of applications in auto industry. Brake pads are an important part of the vehicle's braking system and help reduce speed of vehicle by creating friction between the brake pad and disc (Singh, 2021; Öktem et al., 2021). As it is known asbestos acts as a reinforcing fiber, and is a part of brake pads due to its good thermal conductivity, tribological properties and low cost, however, asbestos had gained widespread acknowledgement as a carcinogen (Chan and Stachowiak, 2004; Talegaonkar and Gopinath, 2009). Consequently, a multitude of several types of brake pads have been developed in the market within the perspective of the post-asbestos brake pad revolution, each having with their own unique composition as the general classification of brake pads has been used in the brake industry. The brake pad's ingredients are generally classified into four categories including polymer binders (10–30 wt%), reinforcing fibers (5–40 wt%), friction modifiers, i.e., solid abrasives and lubricants

(3–35 wt%), and fillers (40–80 wt%) (Akıncioğlu et al., 2021a, 2021b; Chan and Stachowiak, 2004; Kolluri et al., 2010; Kurihara et al., 2012). In addition, the considerations of the environmental issues for the new brake pads are proper significantly important due to the increasing contribution of non-exhaust emissions to air pollution (Ige et al., 2019).

The current trends and future perspective for friction materials used in auto industry should not have asbestos because of its negative influence on human health. Also, copper with a high thermal conductivity is used in auto break manufacture conducting very effectively heat from the friction interface. However, it is a known fact that copper in brake pads has recently become the topic of considerable discussion, primarily due to its potentially toxic effect on human health and the environment along with water quality. The amount of copper in friction materials had been reduced in less than 5 % in 2021, low amount of copper, and it is targeted to have 0.5 % by 2025, practically no use of copper. Therefore, the eco-friendly NAO and copper free brake pads are considered as an alternative option to replace such materials. Carbonaceous materials, i.e., graphite, coke, carbon black and carbon fiber are important

\* Corresponding author.

E-mail address: [chanchira@g.swu.ac.th](mailto:chanchira@g.swu.ac.th) (C. Jubsilp).

<https://doi.org/10.1016/j.arabjc.2024.105769>

Received 23 January 2024; Accepted 29 March 2024

Available online 30 March 2024

1878-5352/© 2024 The Authors. Published by Elsevier B.V. on behalf of King Saud University. This is an open access article under the CC BY-NC-ND license (<http://creativecommons.org/licenses/by-nc-nd/4.0/>).

ingredients which is about 1.25–18 wt% of brake pads for replacement of asbestos and copper (Aranganathan and Bijwe, 2015; Jubsilp et al., 2017; Lertwassana et al., 2012; Lin et al., 2020; Öktem et al., 2021; Straffelini et al., 2015; Wongpayakyotin et al., 2021). The use of carbon fiber as reinforcement to determine the friction performance of the polymer composites has been evaluated. Lertwassana et al., 2019 have reported that the addition of carbon fibers was found to improve wear resistance of the polybenzoxazine friction composites. Jubsilp et al. (2017) also evaluated friction performance of polybenzoxazine friction composites filled with various particle sizes of natural graphite. The results showed that the addition of larger graphite particles can help improve wear resistance, while the coefficient of friction (COF) was increased by the addition of smaller size of graphite particles. In another work, a newly commercialized graphite which is more conducting than the ordinary graphite was evaluated to replace copper in friction materials as the influence of amount of the graphite on tribological properties of phenolic composites for brake shoes were also studied (Aranganathan and Bijwe, 2015). Three composite samples containing all major elements of friction materials were developed having various contents of graphite. It was found that 10 % graphite was observed as an optimum amount resulting in the highest wear resistance and good COF. Öktem et al., 2021 have investigated a new optimized design of brake pad formulation to improve its performance. The formulation was designed by using petro-coke powder acted as a friction modifier to replace of cashew, which is cheaper and more readily available. It was found that petro-coke powder provided a more effective stabilizer for the friction coefficient and improved the specific wear rate. In addition, based on environmental impact, lignocellulosic biomass has been considered as a valuable resource such as graphitic carbon for friction materials (Omran et al., 2016; Sutikno et al., 2010; Xinyu et al., 2014). Sutikno et al., 2010 have evaluated surface roughness, hardness, tensile strength and wear resistance of the friction materials filled with carbonized coconut char powders. They summarized that carbon made from coconut char powders can replace the role of graphite or coal powders as fillers for brake friction materials. Therefore, it is possible that carbonized hemp hurd particles can also be used to replace graphite in the brake friction materials since it has rather high carbon content, i. e., 73.8 – 86.8 % (Marrot et al., 2022) compared with those of carbonized coconut shell, i.e., 49.9 % (Umerah et al., 2020).

In addition, friction material binders would be one area to be investigated. For the binder of brake pads, phenolic is the most commonly used resin, due to its low cost. However, it has some deficiencies, including the use of acid or alkaline catalysts in the synthesis step, the release of water or ammonia as a by-product during the processing, short shelf-life, and brittleness (Ghosh et al., 2007). Moreover, cracks or bulges of molder occurred during a processing due to a gas by-product generated from a curing agent, i.e., hexamethylenetetramine are also some disadvantages of phenolic resins for friction materials (Kurihara et al., 2012). Therefore, there is a need to develop non-phenolic resin binders as alternative materials. The use of polybenzoxazine, a novel type of phenolics, as a binder for friction composite materials has been studied in various past works (Jubsilp and Rimdusit, 2017; Kurihara et al., 2012; Lertwassana et al., 2019; Wongpayakyotin et al., 2021; Wu et al., 2012). It is a fact that the benzoxazine resin can overcome the inherent problems of the phenolic resin as it generates no gas in processing step and could result in a friction composite material with a superb heat resistance and high strength. There is still limited information on using polybenzoxazine and carbonized hemp hurd in production of friction composites. Therefore, the objective of this study was developing eco-friendly friction composites based on polybenzoxazine filled with varying mass ratios of carbonized hemp hurd particles (CHH) and synthetic graphite particles (SG). Also, the effect of carbonized hemp hurd contents on mechanical, thermal and tribological properties of such friction composites was investigated. Finally, a finite element analysis program ANSYS has also been employed for the contact pressure determination as well as wear simulation of the obtained

polybenzoxazine friction composites within the scope of this study.

## 2. Materials and methods

### 2.1. Materials

Benzoxazine resin (BA-35x) was based on bisphenol-A obtained from PTT Phenol Co., Ltd. (Rayong, Thailand), paraformaldehyde purchased from Merck Co., Ltd. (Darmstadt, Germany) and 3,5-xylydine purchased from Panreac Quimica SA. (Barcelona, Spain). Carbon fiber and glass fiber were obtained from SJ Sinhuphun Trading Co., Ltd. (Bangkok, Thailand) and Toho Beslon Co., Ltd. (Tokyo, Japan) respectively. Aramid pulp was supplied by Du Pont (Tokyo, Japan). Iron fibers, synthesis graphite ( $\rho = 2.18 \text{ g/cm}^3$ ), zirconium silicate, barium sulfate, NBR and cashew dust were provided by Compact International Co., Ltd. (Phetchaburi, Thailand). Carbonized hemp hurd ( $\rho = 1.69 \text{ g/cm}^3$ ) were supplied by Highland Research and Development Institute (Chiang Mai, Thailand). All the chemicals for the experiment were used without purification.

### 2.2. Preparation of BA-35x and CHH

BA-35x was synthesized by using bisphenol-A, paraformaldehyde and 3,5-xylydine at a molar ratio of 1:4:2 at a temperature of 110 °C for 40 min (Ishida, 1996). The light clear-yellowish solid resin was obtained at room temperature and the solid resin was then ground to fine powder and kept in a refrigerator for future-use.

Carbonized hemp hurd particles (CHH) were prepared by milling from carbonized hemp hurd. The fractions of the CHH sizes that pass through a sieve were similarly designed to commercial synthetic graphite particles (SG). The CHH were dried at a temperature of 105 °C for 24 h and kept in the desiccator before use. The elemental composition (wt %) was analyzed by ultimate analysis of CHH: C = 65.37, H = 3.48, N = 0.80, S = 0.16 and O = 19.57.

### 2.3. Preparation of SG/CHH-filled poly(BA-35x) composite samples

The SG/CHH-filled poly(BA-35x) composite samples are formulated from 10 to 11 ingredients in four categories as listed in Table 1. The various contents of SG and CHH, SG/CHH (wt%/wt%), are SG/CHH (10/0), SG/CHH (8/2), SG/CHH (6/4), SG/CHH (4/6), SG/CHH (2/8) and SG/CHH (0/10). The molding compounds from all ingredients were mechanically mixed at about 120 °C for 45 min. Then, the compounds were thermally cured at a temperature of 200 °C for 2 h by a compression-molder under a hydraulic pressure of 15 MPa. The fully cured composite samples was obtained after air-cooled in room

**Table 1**  
The ingredients and compositions of polybenzoxazine composite samples.

Function	Ingredients	Avg. particle size/ Avg. fiber diameter ( $\mu\text{m}$ )	Composition (wt%)
Binder	Benzoxazine resin (BA-35x)		10
Reinforcing fibers	Aramid pulp	0.37	3.75
	Carbon fiber	9.5	1.25
	Glass fiber	16.4	10
	Iron fiber	58	25
Friction modifiers	Zirconium silicate	3.3	7
	Synthetic graphite (SG)	1.5	10/8/6/4/2/0
	Carbonized hemp hurd (CHH)	20–150	0/2/4/6/8/10
Fillers	Barium sulphate	6.2	25
	NBR	3.2	4
	Cashew dust	23	4

temperature before their characterizations. Some examples of the composite samples are presented in Fig. 1.

#### 2.4. Characterizations of the samples

Mechanical properties of the samples were measured on Universal Testing Machine, Instron 5567 (United State) using three-point bending mode. The dimensions of sample are 25 mm × 60 mm × 3 mm. The support span is 48 mm, and a crosshead speed is 2 mm/min according to ASTM D790. Five replicas were used for evaluation of mechanical properties.

Functional groups of the samples were studied using a spectrum GX FT-IR spectrometer from Perkin Elmer with an ATR accessory (Waltham, MA, USA). All spectra were taken as a function of time with 32 scans at resolution of 4 cm<sup>-1</sup> and wavenumber ranging from 4000 to 400 cm<sup>-1</sup>. Three samples were repeated to confirm the findings.

Storage modulus ( $E'$ ) and loss tangent ( $\tan \delta$ ) of the samples were carried out using Dynamic Mechanical Analyzer, DMA1, Mettler Toledo (Switzerland). The dimensions of sample are 10 mm × 50 mm × 2.5 mm. The sample was measured by three-point bending mode at a frequency of 1 Hz with a heating rate of 2 °C/min from 30 °C to 300 °C under nitrogen atmosphere. Three samples were repeated to confirm the findings.

Thermal stabilities, i.e., degradation temperature at 5 % weight loss ( $T_{d5}$ ) and residual weight of the samples were studied under dynamic conditions using a thermogravimetric analyzer TGA1, Mettler Toledo (Switzerland). The sample about 10 mg was operated at a heating rate of 20 °C/min from 30 °C to 1000 °C in nitrogen gas flow 50 ml/min. Each sample was repeated three times.

The worn surface of the sample was analyzed by scanning electron microscope (SEM), model JEOL JSM-6510 from JEOL Ltd. (Tokyo Japan) with an acceleration voltage of 5 kV. Each sample was given a thin layer of gold film using a sputter coater, model SCD 040 from Oerlikon Balzers Coating (Thailand) Co., Ltd. (Chonburi, Thailand).

Coefficient of friction (COF) of the sample at a room temperature of 25 °C was performed by a ball-on-disc tribometer (shown in Fig. 2(a)), CSM TRB-S-DE, Anton Paar (Australia) under dry sliding with a speed range of 0.366 m/s and a load of 10 N. The sliding distance of 1000 m was measured to obtain steady-state values of coefficient of friction (COF) of the samples. Material of testing balls is carbon steel. The COF of each sample was averaged of triplicate measurements.

Coefficient of friction (COF) and specific wear rate ( $V$ ) of the sample as a function of temperature were determined from a constant speed brake lining tester, HP-8-LC (Tokyo, Japan) (shown in Fig. 2(b)) at test temperature levels of 100, 150, 200, 250, 300, and 350 °C according to TIS97-2557 which is similar to JIS-D4411 and GB5763-2008. The



Fig. 1. Some examples of fully cured SG/CHH -filled poly(BA-35x) composite samples.

material of disc is grey cast iron. The sample size is 25 mm × 25 mm × 7 mm and the test conditions are listed in Table 2.

The  $V$  of the sample as a function of temperature was also calculated as follows equation (1).

$$V = \frac{1}{2\pi R} \times \frac{A}{n} \times \frac{d_1 - d_2}{f_m} \quad (1)$$

where,  $V$  is specific wear rate (cm<sup>3</sup>/Nm),  $R$  is distance between the center of the sample and the center of rotation axis (150 mm),  $n$  is total number of rotations of disc during the wearing test,  $A$  is total frictional area of the sample (mm<sup>2</sup>),  $d_1$  is average thickness of the sample before testing (mm),  $d_2$  is average thickness of the sample after testing (mm), and  $f_m$  is total average frictional force in testing period (N). The COF and  $V$  of each sample was averaged of two pieces.

#### 2.5. Finite element analysis of disc brake system

The disc brake model (3D) consisted of disc and pad were designed in Design Modeller and their 3D solid model were analyzed by ANSYS Workbench 2022 R1 software, Ansys, Inc. Houston, USA. A 3D mesh was crated with tetrahedral 3D elements. The number of elements and nodes of the disc brake model are 39,208 and 20,351, respectively. Gray cast iron disc and pads (SG/CHH-filled poly(BA-35x) composite samples) were homogeneous and the pads were considered to be an isotropic elastic materials. The mechanical properties of the disc and the pads are listed in Table 3. Static structural simulation was chosen to analyze mechanical contact-brake disc pad. The total simulation time for braking was  $t = 673$  s, the following initial time steps, and the structural boundary conditions applied to the pad are tabulated in Table 4. The calculation related to the contact pressure on the disc was determined.

#### 2.6. Wear rate simulation

Wear predictions of the pad's surface due to removal materials can be also solved by finite element analysis program, ANSYS. A generalized form of Archard's wear law as given by equation (3) is proposed to predict wear in sliding contacts between disc and pad for disc brake system. It is assumed that the wear rate at any point on the contact surface is proportional to the normal contact pressure ( $p$ ) and the relative sliding velocity ( $v$ ). Moreover, the equation (3) can be reformulated as presented in equation (4).

$$\frac{dh}{dt} = kp v \quad (3)$$

$$\frac{dh}{ds} = kp \quad (4)$$

where  $h$  is the wear depth (m),  $k$  is the dimensional wear coefficient (Pa<sup>-1</sup>),  $p$  is the normal contact pressure (Pa) and  $s$  is the sliding distance.

A wear simulation procedure proposed by Pödra and Andersson, 1999 has been adopted in which the contact pressure distribution is computed by using the finite element analysis. With the obtained distribution, the wear of the brake pad is computed by numerical integration of equation (4) according to the explicit Euler integration scheme using the mathematical programming language MATLAB. The procedure is implemented in ANSYS and looped through a series of static structural analyses of the finite element model, each with an updated geometry of the pad surface. Each step starts with a static structural analysis that computes the nodal contact pressure at each of the surface nodes (Söderberg and Andersson, 2009). The wear depth at node number  $i$  after the  $j$ th simulation step is,

$$h_{i,j} = h_{i,j-1} + \Delta h_{i,j}$$

$$\Delta h_{i,j} = kp_{i,j} \Delta s_{i,j}$$

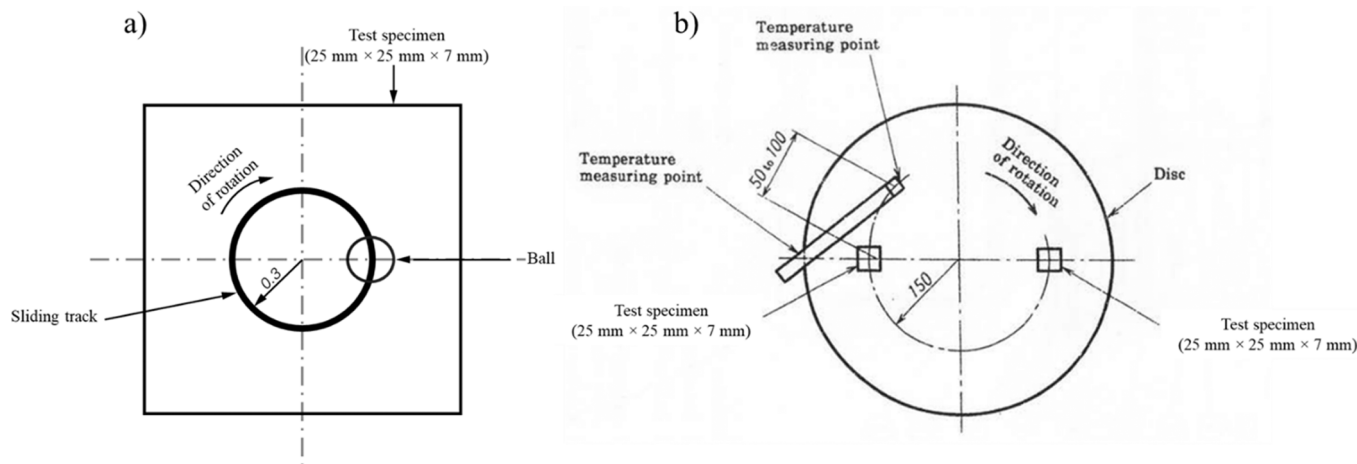


Fig. 2. (a) A ball-on-disc tribometer (b) The constant speed brake lining tester.

Table 2

The test conditions according to TIS97-2557: Brake linings for vehicles.

Test conditions	
The tolerance on test temperature	$\pm 10$ °C
The sliding speed of frictional surface of disc against test sample	A constant speed given within 6 m/s to 8 m/s
The pressing pressure of test sample	$1 \pm 0.02$ MPa
The direction of friction	The direction of friction at the time of the use of lining

Table 3

Mechanical properties of disc and brake pads (SG/CHH-filled poly(BA-35x) friction pads).

Property	Disc <sup>a</sup>	SG/CHH (10/0)-filled poly(BA-35x) Pad	SG/CHH (2/8)-filled poly(BA-35x) Pad
		Young's modulus, $E$ (GPa)	138
Poisson's ratio, $\nu$	0.3	0.25 <sup>a</sup>	0.25 <sup>a</sup>
Density, $\rho$ (kg/m <sup>3</sup> )	7250	2420	2300
Coefficient of friction, COF		0.35 (100 °C)	0.43 (100 °C)
		0.37 (150 °C)	0.43 (150 °C)
		0.38 (200 °C)	0.41 (200 °C)
		0.38 (250 °C)	0.40 (250 °C)
		0.37 (300 °C)	0.43 (300 °C)
		0.37 (350 °C)	0.42 (350 °C)

<sup>a</sup> data from Belhocine and Omar, 2016.

where  $h_{i,j-1}$  is the wear depth after the  $(j - 1)$ th step,  $\Delta h_{i,j}$  is the incremental nodal wear depth during the  $j$ th step,  $p_{i,j}$  is the nodal pressure, and  $\Delta s_{i,j}$  is the incremental nodal sliding distance.

The incremental sliding distance of a node on the pad surface is proportional to its radial distance from the center of the rotor according to  $\Delta s_{i,j} = n_j 2\pi r_i$ , where  $n_j$  is number of rotor revolutions during the  $j$ th step and  $r_i$  is number of rotor revolutions during the  $j$ th step.

### 3. Results and discussion

#### 3.1. Flexural properties of SG/CHH-filled poly(BA-35x) composite samples

The effect of CHH contents on flexural properties of poly(BA-35x) composites filled with SG/CHH of 10/0, 8/2, 6/4, 4/6, 2/8, and 0/10 (wt%/wt%) is depicted in Fig. 3. The flexural strength and modulus of the SG/CHH-filled poly(BA-35x) composites enhanced by an addition of the CHH content, i.e., from 43.2 MPa to 52.0 MPa and from 7.0 GPa to

Table 4

The structural boundary conditions applied to the brake pads of SG/CHH-filled poly(BA-35x) friction pads filled with 0 wt% and 8 wt% CHH.

Conditions	SG/CHH (10/0)-filled poly(BA-35x) Pad	SG/CHH (2/8)-filled poly(BA-35x) Pad
Wear coefficient ( $\text{Pa}^{-1}$ )	$1.43 \times 10^{-14}$ (100 °C)	$1.30 \times 10^{-14}$ (100 °C)
	$1.58 \times 10^{-14}$ (150 °C)	$1.34 \times 10^{-14}$ (150 °C)
	$1.67 \times 10^{-14}$ (200 °C)	$1.56 \times 10^{-14}$ (200 °C)
	$1.92 \times 10^{-14}$ (250 °C)	$1.78 \times 10^{-14}$ (250 °C)
	$2.15 \times 10^{-14}$ (300 °C)	$1.92 \times 10^{-14}$ (300 °C)
	$3.59 \times 10^{-14}$ (350 °C)	$3.59 \times 10^{-14}$ (350 °C)
Pressure of piston pad (MPa)	1	
Constant angular velocity (rad/s)	46.67	
Mesh	Tetrahedral 3D elements	
Formulation	augmented Lagrangian method	
Relevance	100	
Fixed support	Finger pad	
Temperature	100–350 °C	
Revolutions (rounds)	5,000	
Radius (m)	0.15	
Simulation time for braking (s)	673	
Increment of initial time (s)	0.25 <sup>b</sup>	
Increment of minimal initial time (s)	0.125 <sup>b</sup>	
Increment of maximal initial time (s)	0.5 <sup>b</sup>	

<sup>b</sup> data from Belhocine and Omar, 2016.

9.0 GPa, respectively, for SG/CHH from 10/0 to 0/10. In general, the strength and modulus of reinforced composites mainly depends on the properties of their ingredients and interfacial adhesion between the filler and the matrix. Therefore, except the properties of their ingredients of the poly(BA-35x) composites, the improvement of strength of the composites suggested that the addition of the CHH could enhance the CHH-poly(BA-35x) interfacial adhesion because the poly(BA-35x) chains could go into the honeycomb-like pore structures of CHH (Fig. 4(b)), leading to better stress transfer efficiency from the poly(BA-35x) and CHH as can be seen the fractured surface in Fig. 4(c) which the good interfacial adhesion (green ambits) and the cohesive fracture surface developed in the poly(BA-35x) matrix region (red ambits) could be observed. While the SG-poly(BA-35x) interfacial adhesion showed at the outer surface of the SG only (white ambits) as presented in Fig. 4(f). Good CHH-poly(BA-35x) interfacial adhesion observed in Fig. 4(c) also

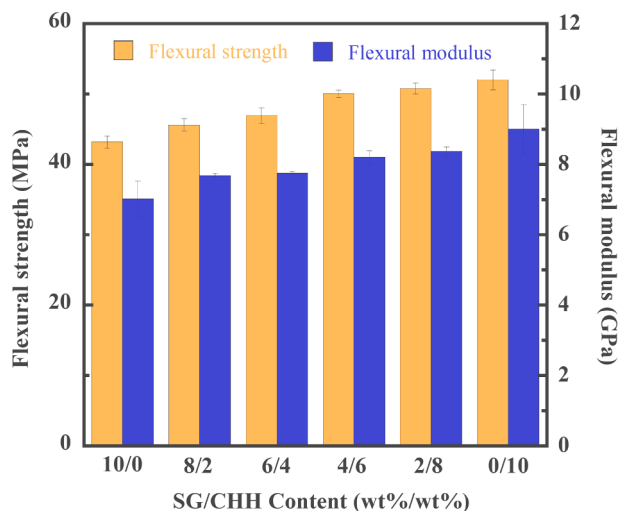


Fig. 3. Flexural properties of SG/CHH-filled poly(BA-35x) composite samples at various SG/CHH contents.

resulted in the motion of the poly(BA-35x) chain restricted by CHH and the composites became increasing modulus. Moreover, it was remarked that the rather high flexural properties of the SG/CHH-filled poly (BA-35x) composite were obtained when compared with other polymer composites for friction materials, i.e., strength of 10.0–40.0 MPa and modulus of 3.0–8.0 GPa under flexure loading (Mathur et al., 2004).

### 3.2. Network formation of SG/CHH-filled poly(BA-35x) composite samples

To confirm the formation of an interfacial adhesion between CHH and poly(BA-35x) that resulted in an enhancement of mechanical property of the composite samples as above mentioned, FTIR spectroscopy was performed on the CHH, SG, poly(BA-35x), CHH-filled poly(BA-35x) composite sample and SG-filled poly(BA-35x) composite sample to determine the presence of the functional groups on them as can be seen

in Fig. 5. Fig. 5(a), FTIR spectra of CHH shows the broad absorption band in a range of 3500–3000  $\text{cm}^{-1}$  attributed to free and associated hydroxyl groups and structural hydroxyl groups ( $-\text{COOH}$  and  $-\text{COH}$ ). The absorption bands at 1587  $\text{cm}^{-1}$  (C = O stretching mode of conjugated ketones and quinones), 1380  $\text{cm}^{-1}$  ( $\text{CH}_2$  units in biopolymers), 832–600  $\text{cm}^{-1}$  (C–H bond in aromatic and heteroatomic compounds) were detected (Sahoo et al., 2021; Srinivasan et al., 2015). In addition, the absorption band at 1300–1000  $\text{cm}^{-1}$  ascribed to the glycosidic bond was also observed (He et al., 2022). While, in Fig. 5(b), FTIR spectra of SG displays very less functional group as SG were characterized by a very well assembled layer of carbon. In case of poly(BA-35x), Fig. 5(c) indicates the absorption bands of the poly(BA-35x) after oxazine ring of BA-35x resin was opened by thermal polymerization, i.e., 3300  $\text{cm}^{-1}$  (hydroxy groups), 1488  $\text{cm}^{-1}$  (tetra-substituted aromatic ring) and 1240–1020  $\text{cm}^{-1}$  (asymmetric C–N–C stretching) (Jubsilp et al. (2018)).

For the FTIR spectra of CHH-filled poly(BA-35x) composite sample as plotted in Fig. 5(d), it was observed that the intensity of an absorption band at 3300  $\text{cm}^{-1}$  of the poly(BA-35x) was quietly increased. This behavior may be the effect from hydroxyl groups of the CHH. In addition, it is possible that the OH groups of the poly(BA-35x) can be further interacted with the OH groups and C = O groups of the CHH to form hydrogen bonding (H-bonding) as can be seen the new absorption band at 1720  $\text{cm}^{-1}$  and the disappearance of the absorption band at 1587  $\text{cm}^{-1}$  of the CHH (Guo et al., 2010; Rimdusit et al., 2006, 2007). In case of SG-filled poly(BA-35x) composite sample as depicted in Fig. 5(e), it was observed that the intensity of an absorption band at 3300  $\text{cm}^{-1}$  of poly(BA-35x) was similar to that of the poly(BA-35x) due to no H-bonding formation as expected.

### 3.3. Thermomechanical properties of SG/CHH-filled poly(BA-35x) composite samples

Thermomechanical properties, i.e., storage modulus ( $E'$ ) and loss tangent ( $\tan \delta$ ) at a different of temperature of the poly(BA-35x) composite samples filled with SG/CHH of 10/0, 8/2, 6/4, 4/6, 2/8, and 0/10 (wt%/wt%) were determined by dynamic mechanical analysis as illustrated in Fig. 6. The  $E'$  represents the energy stored in the samples following deformation under load at various temperature, and related to

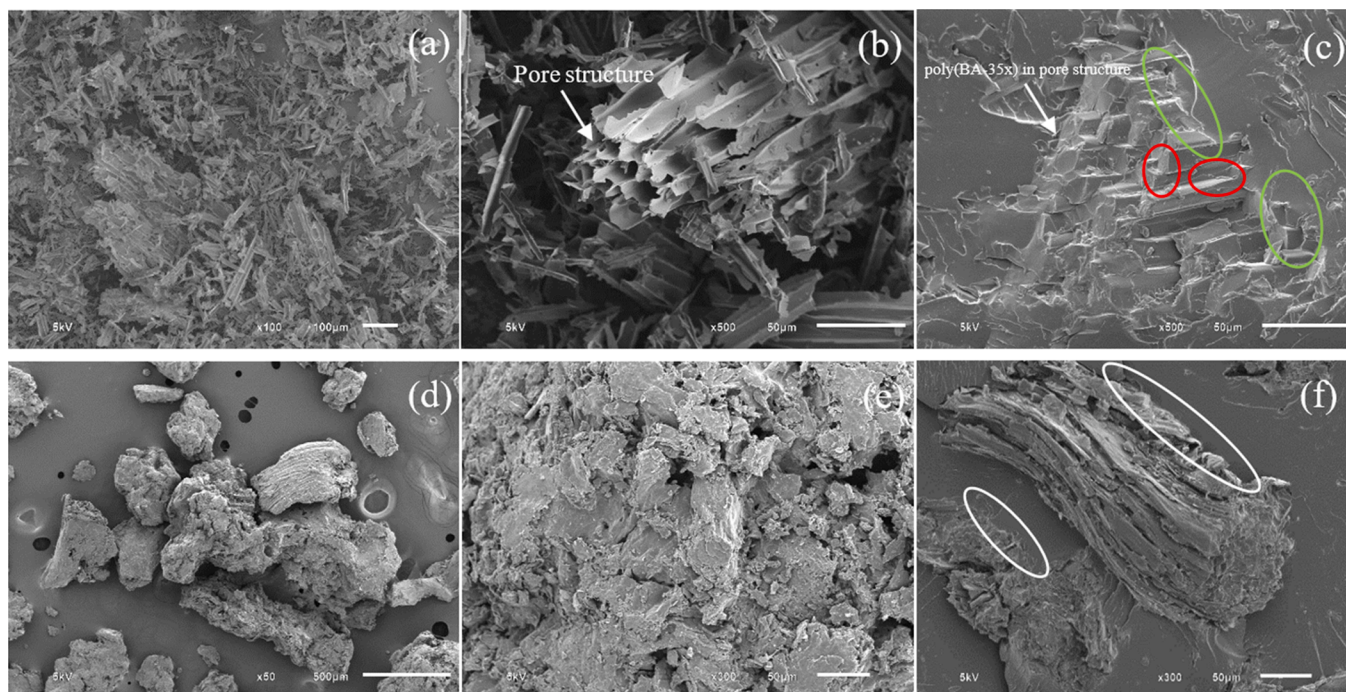


Fig. 4. SEM micrographs (a,b) CHH particles (c) 10 wt% CHH-filled poly(BA-35x) composite (d,e) SG particles (f) 10 wt% SG-filled poly(BA-35x) composite.

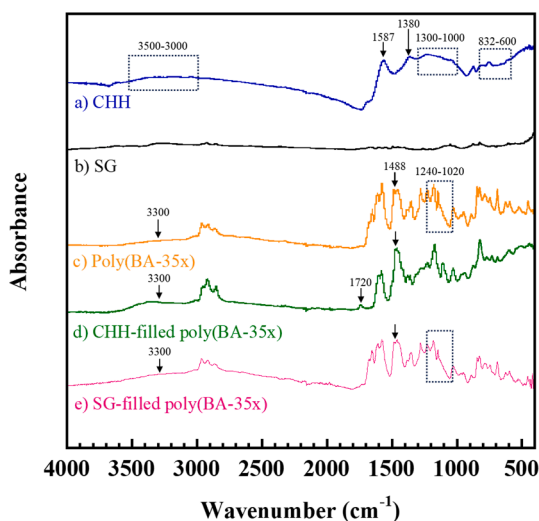


Fig. 5. FTIR spectra of (a) CHH (b) SG (c) poly(BA-35x) (d) CHH-filled poly(BA-35x) composite sample (e) SG-filled poly(BA-35x) composite sample.

their stiffness which is one of the key parameters representing for COF and wear rate (Ahmadijokani et al., 2019; Wongpayakyotin et al., 2021; Wu et al., 2012).

From Fig. 6(a), the  $E'$  at glassy state (50 °C) of the poly(BA-35x) composites filled with SG/CHH from 10/0 to 0/10 (%wt%/wt%) were found to be 4.93, 5.03, 5.18, 5.42, 5.51, and 5.64 GPa, respectively. In addition, their rubbery plateau modulus was also found improved with increasing CHH content. The increase in modulus could be also explained by the hydroxyl groups in the CHH that could react with the poly(BA-35x) to form significantly strong H-bonding, in consequence, the crosslink density increased. Moreover, the poly(BA-35x) composites filled with higher CHH contents showed more relative dimensional stability as it can be observed that the SG/CHH (10/0)-filled poly(BA-35x) composite sample showed stability of  $E'$  at approximately 150 °C and then tended to significantly decrease as the thermal glass-rubber transition occurred. While, the  $E'$  of the SG/CHH (0/10)-filled poly(BA-35x) composite sample was stable even when the temperature was up to 200 °C and the gradual decrease of the  $E'$  of the composite sample was then observed.

Fig. 6(b) is a plot of  $\tan \delta$  at a different of temperature of the poly(BA-35x) composites filled with SG/CHH from 10/0 to 0/10 (wt%/wt%).

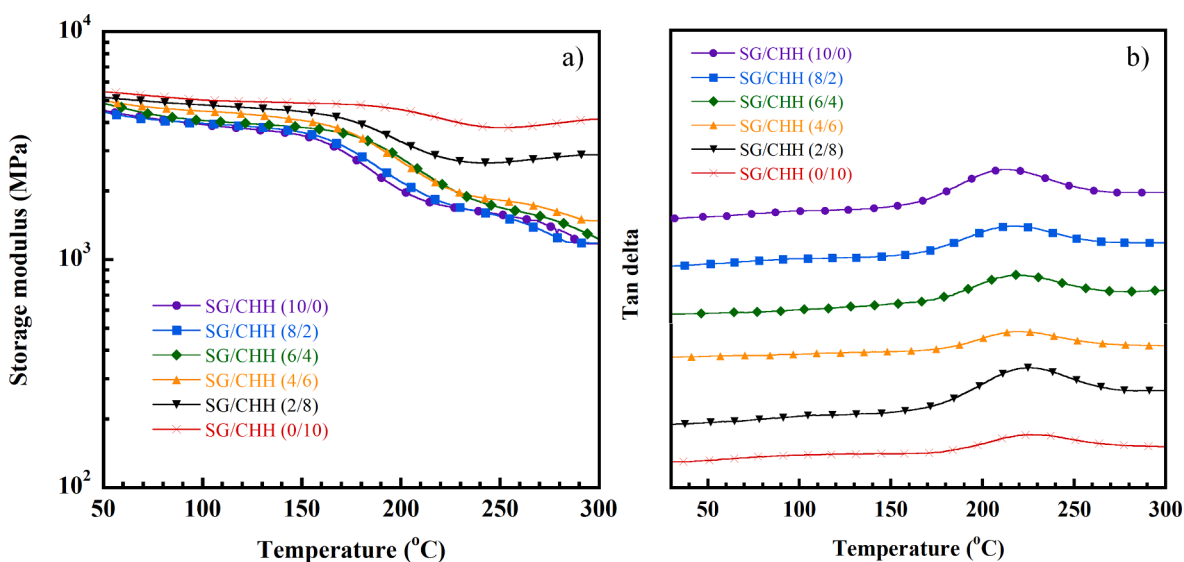


Fig. 6. (a) Storage modulus, (b)  $\tan \delta$  of SG/CHH-filled poly(BA-35x) composite samples at various SG/CHH contents.

The temperature at the  $\tan \delta$  peak was used to represent the glass transition temperature ( $T_g$ ) of the composite samples. The  $T_g$  is described as a polymer change from a glassy state to a rubbery soft state related to 30–50 carbon chains start to move at the  $T_g$ . From the same figure, the  $\tan \delta$  peak of the SG/CHH-filled poly(BA-35x) composite samples was systematically shifted to higher temperature, i.e., 212, 215, 218, 222, 225, and 228 °C, respectively, with an increase of the CHH content from 0 wt% to 10 wt%. This performance indicates CHH filler-like effect to be more dominant with increase in the CHH to SG mass ratio, resulting in increased crosslinking density from the interfacial bonding formation between the hydroxyl groups in the CHH and the poly(BA-35x) which required more energy to transform from the glassy state to the rubbery state of the SG/CHH-filled poly(BA-35x) composite samples as similar characteristic discussed in high performance friction materials of aramid pulp/carbon fiber-reinforced polybenzoxazine composites (Lertwassana et al., 2019). It would be expected that the SG/CHH-filled poly(BA-35x) composite samples with higher  $T_g$  can provide wear performance better than those same type of composite samples with lower  $T_g$  as previously informed by Wu et al., 2012 and Wongpayakyotin et al., 2021.

### 3.4. Thermal stabilities of SG/CHH-filled poly(BA-35x) composite samples

As it is known that breaking may rise the temperature at the disc-pad interface up to 800 °C in severe conditions (Ahmadijokani et al., 2019; Hwang et al., 2010). Therefore, practical performances of polymer composite friction materials can be provided by one of crucial key parameters that is thermal stability. TGA thermograms of SG/CHH-filled poly(BA-35x) composite samples at SG/CHH contents from 10/0 to 0/10 (wt%/wt%) are depicted in Fig. 7(a). Three main degradation steps of the SG/CHH-filled poly(BA-35x) composite samples were observed. The first degradation step was found in the range of 250–500 °C corresponding to the degradation of cashew dust, NBR powder and poly(BA-35x) (Lertwassana et al., 2019). The second degradation step took place the onset temperature from 500 °C to 600 °C displaying the degradation of aramid pulp (Lertwassana et al., 2019; Liu and Yu, 2006) and CHH (Matykiewicz, 2020). The onset and offset temperatures of the third degradation step were observed at approximately 600 °C and 900 °C, respectively, related to degradation of barium sulphate zirconium silicate, synthetic graphite, carbon fiber and iron fiber (Ahmadijokani et al., 2019; Lertwassana et al., 2019).

In addition, the degradation temperature at 5% weight loss ( $T_{d5}$ ) and

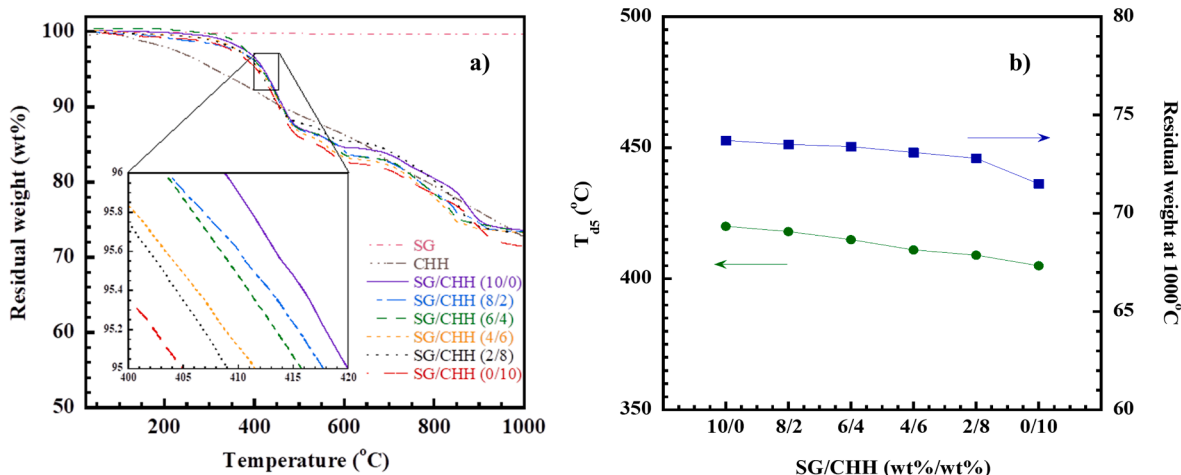


Fig. 7. (a) TGA thermograms of SG/CHH-filled poly(BA-35x) composite samples at various SG/CHH contents, CHH and SG (b)  $T_{d5}$  and residual weight at 1000 °C of SG/CHH-filled poly(BA-35x) composite samples at various SG/CHH contents.

residual weight at 1000 °C of the SG/CHH-filled poly(BA-35x) composite samples was analyzed and depicted in Fig. 7(b). It was observed in the inserted figure that a decrease of CHH content was found to promote the  $T_{d5}$  and residual weight of the SG/CHH-filled poly(BA-35x) composite samples. The  $T_{d5}$  was 420, 418, 415, 411, 409, and 404 °C and the residual weight was 73.7, 73.5, 73.4, 73.1, 72.8, and 71.5 % for an addition of SG/CHH from 10/0 to 0/10 (wt%/wt%), respectively. This behavior is possible that  $T_{d5}$  (>1000 °C) and residual weight (~99.0 % at 1000 °C) of the SG was relatively higher than that  $T_{d5}$  (330 °C) and residual weight (75.0 % at 1000 °C) of the CHH. However, under nitrogen atmosphere, the  $T_{d5}$  and residual weight at 1000 °C of all SG/CHH-filled poly(BA-35x) composite samples exhibited higher values than  $T_{d5}$  (~350–400) and residual weight at 1000 °C (65–70 %) of the phenolic type samples which are widely used as commercial friction materials (Ahmadijokani et al., 2019; Bashir et al., 2021). Therefore, it is possible that higher residual weight of the SG/CHH-filled poly(BA-35x) composite samples than that of the phenolic type samples could limit the exothermicity of the pyrolysis reactions, decrease the production of volatile gases and inhibit the thermal conduction of composites.

### 3.5. Tribological properties of SG/CHH-filled poly(BA-35x) composite samples

Tribological responses and performances of friction materials could be measured through COF. Fig. 8 indicates COF at room temperature of 25 °C within the sliding distance of 1000 m of SG/CHH-filled poly(BA-35x) composite samples at SG/CHH contents from 10/0 to 0/10 (wt %/wt%). The COF of the SG/CHH-filled poly(BA-35x) composite samples were 0.30, 0.31, 0.32, 0.34, 0.36, and 0.38 for SG/CHH contents from 10/0 to 0/10 (wt%/wt%), respectively. The increment of the COF of the SG/CHH-filled poly(BA-35x) composite samples with increasing CHH content is possible that shear stresses may promote the disintegration of the CHH at the glycosidic bond and weaken the stress absorbing capacity of the composite with higher CHH content, resulting in the higher COF as similarly explained in the composite filled with cellulose fiber (Satapathy and Bijwe, 2004).

### 3.6. Tribological properties at 100 °C–350 °C of SG/CHH-filled poly(BA-35x) composite samples

From above-mentioned results, it was found that the addition of SG/CHH 2/8 (wt%/wt%) for poly(BA-35x) composite sample had a balance of properties, including COF, mechanical properties, and temperature resistance so that the composite sample can be considered to evaluate the COF and specific wear rate as a function of temperature.

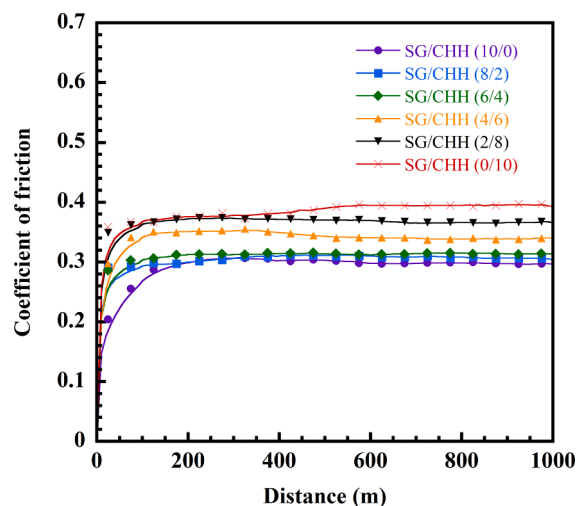


Fig. 8. Coefficient of friction in a distance of 1000 m of SG/CHH-filled poly(BA-35x) composite samples at various SG/CHH contents.

The effect of temperature on COF and specific wear rate of the SG/CHH (2/8)-filled poly(BA-35x) composite sample was evaluated to compare with those of the SG/CHH (10/0)-filled poly(BA-35x) composite sample, NAO friction phenolic composite, and asbestos-based commercial brake pad as plotted in Fig. 9(a) and Fig. 9(b), respectively. The COF values at 100 °C–350 °C of the SG/CHH (2/8)-filled poly(BA-35) composite sample, i.e., 0.40–0.43 was relatively higher than that of the SG/CHH (10/0)-filled poly(BA-35x) composite sample, i.e., 0.35–0.38, the NAO friction phenolic composite, i.e., 0.37–0.45, and the asbestos-based commercial brake pad, i.e., 0.36–0.41. Such finding confirms that the addition of the CHH can help enhance COF of the SG/CHH-filled poly(BA-35x) composite sample. In addition, the obtained COF of the SG/CHH-filled poly(BA-35x) composite samples was in the range of 0.2–0.7 at temperature levels of 100 °C–350 °C according to TIS97-2557: Brake linings for vehicles. Furthermore, the SG/CHH (2/8)-filled poly(BA-35x) composite sample showed a more stable COF against the different temperatures compared with the NAO friction phenolic composite and the asbestos-based one. This behavior is possible that the thermal stability of the poly(BA-35x) matrix is higher than that phenolic which is a matrix for the NAO friction composite and the asbestos-based brake pad (Jubsilp et al., 2021).

For specific wear rates, the addition of the CHH in the SG/CHH-filled poly(BA-35x) composite sample also showed an improvement of wear

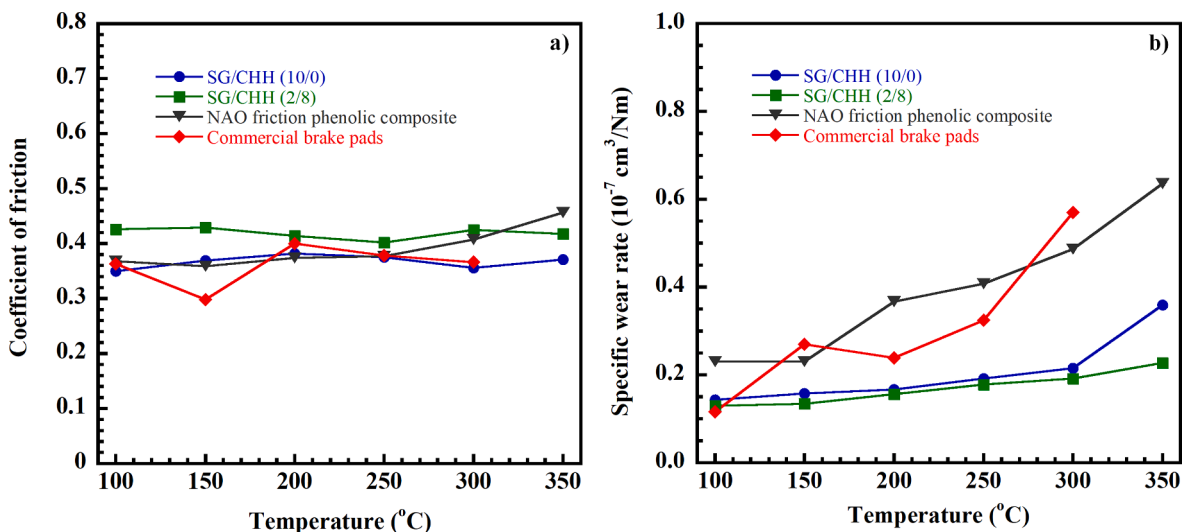


Fig. 9. (a) Coefficient of friction and (b) specific wear rate as a function of temperature of SG/CHH -filled poly(BA-35x) composite samples, NAO friction phenolic composite, and asbestos-based commercial brake pad.

resistance when compared with the poly(BA-35x) composite sample unfilled CHH. It is possible that the higher  $T_g$  of the SG/CHH (2/8)-filled poly(BA-35x) composite sample can help it to retard softening (deformation). This in turn caused slower damage of the sample surface that

eventually leads to generate small amount of wear debris. In comparison with the NAO and the asbestos ones, the SG/CHH (2/8)-filled poly(BA-35x) composite sample showed more wear resistance. This is may be due to significant interfacial adhesion between poly(BA-35x) and all

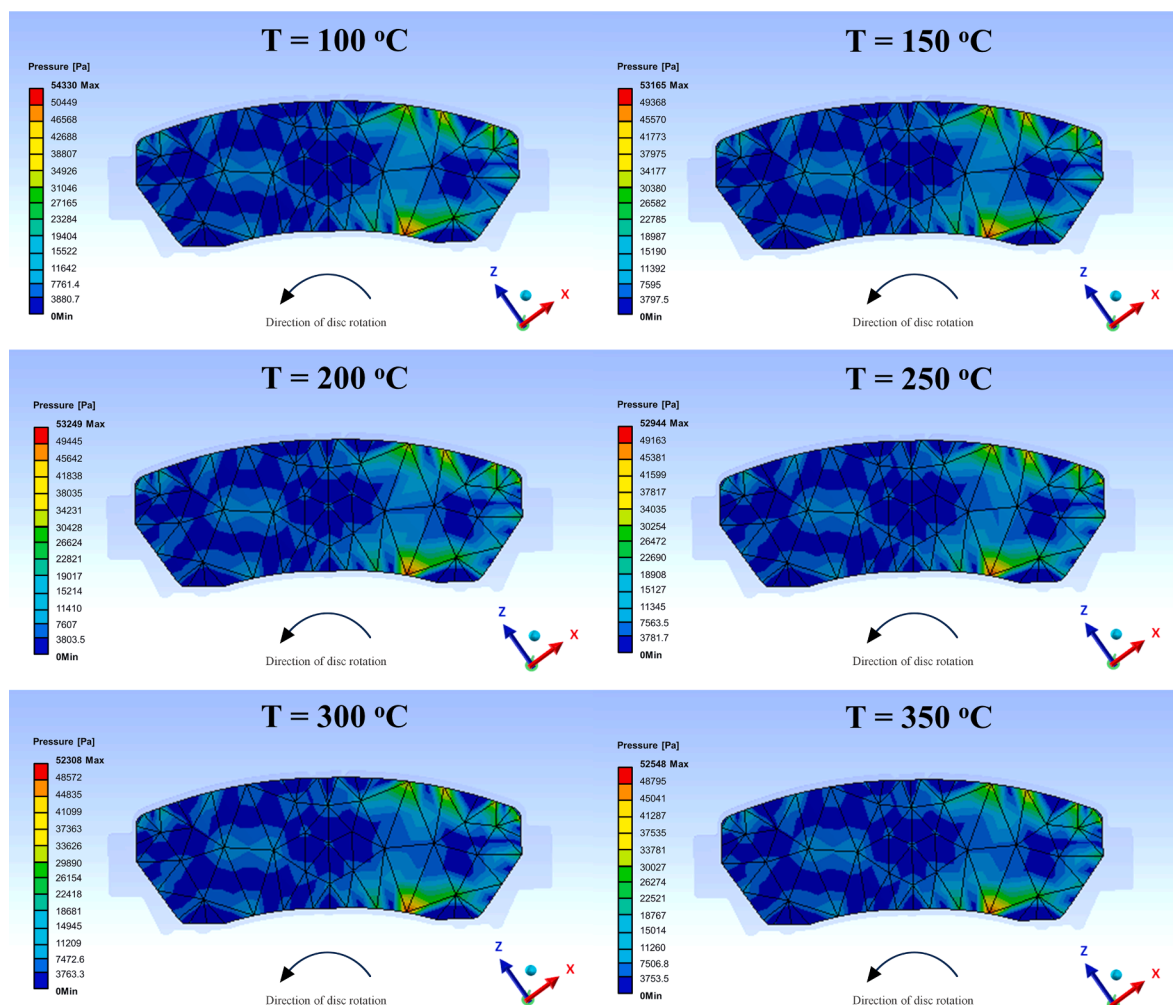


Fig. 10. Interface contact pressure distribution on SG/CHH (2/8)-filled poly(BA-35x) friction pad at 100 °C-350 °C.

ingredients, in consequence, a wear mechanism obtained from the development of friction force at the sliding surface of the SG/CHH (2/8)-filled poly(BA-35x) composite sample was different from that of the NAO and the asbestos ones.

### 3.7. Simulation of wear and contact pressure distribution of SG/CHH-filled poly(BA-35x) friction pads

Wear simulation and its effect on contact pressure distribution at the interface of SG/CHH-filled poly(BA-35x) friction pads and disc of disc brakes was studied by finite element analysis (FEA). In this work, the validity of the analyses in the FEA was evaluated by repetition following the previous work (Belhocine and Omar, 2016). In the FEA simulation, the initial parameters listed in Table 3 and Table 4 were used. From the simulation, the contours of the contact pressure distribution of the poly(BA-35x) friction pads filled with SG/CHH (2/8) and SG/CHH (10/0) at 100 °C-350 °C is presented in Fig. 10 and Fig. 11, respectively. In addition, experimental numerical data of COFs and simulated maximum contact pressure at 100 °C-350 °C of the poly(BA-35x) friction pads are displayed in Table 5 and Table 6. From Fig. 10 and Fig. 11, it was observed that the contours of the contact pressure distribution of both SG/CHH-filled poly(BA-35x) friction pads was quietly similar and tended toward the leading edge of the contact due to the induced frictional traction and the maximum contact pressure was at the edge of the friction pads. The maximum contact pressure at 100 °C-350 °C of the SG/CHH (2/8)- and SG/CHH (10/0)-filled poly(BA-35x) friction pads was in a range of 52.31–54.33 kPa and 54.13–54.95 kPa, respectively. It

**Table 5**

Tribological property of SG/CHH (2/8)-filled poly(BA-35x) friction pad at difference temperature.

Temperature (°C)	COF	Max. contact pressure (kPa)	$V_{\text{Experimental}}$ ( $10^{-7} \text{ cm}^3/\text{Nm}$ )	$V_{\text{FEA Simulation}}$ ( $10^{-7} \text{ cm}^3/\text{Nm}$ )	Difference (%)
100	0.426	54.33	0.130	0.131	1.1
150	0.429	53.17	0.134	0.133	1.1
200	0.414	53.25	0.156	0.155	0.9
250	0.402	52.94	0.178	0.175	1.5
300	0.425	52.31	0.192	0.187	2.7
350	0.418	52.55	0.227	0.222	2.2

**Table 6**

Tribological property of SG/CHH (10/0)-filled poly(BA-35x) friction pad at difference temperature.

Temperature (°C)	COF	Max. contact pressure (kPa)	$V_{\text{Experimental}}$ ( $10^{-7} \text{ cm}^3/\text{Nm}$ )	$V_{\text{FEA Simulation}}$ ( $10^{-7} \text{ cm}^3/\text{Nm}$ )	Difference (%)
100	0.350	54.80	0.143	0.146	1.9
150	0.369	53.13	0.158	0.156	1.2
200	0.382	53.67	0.167	0.163	0.2
250	0.375	54.95	0.192	0.196	2.2
300	0.356	54.33	0.215	0.217	1.1
350	0.371	54.55	0.359	0.357	0.6

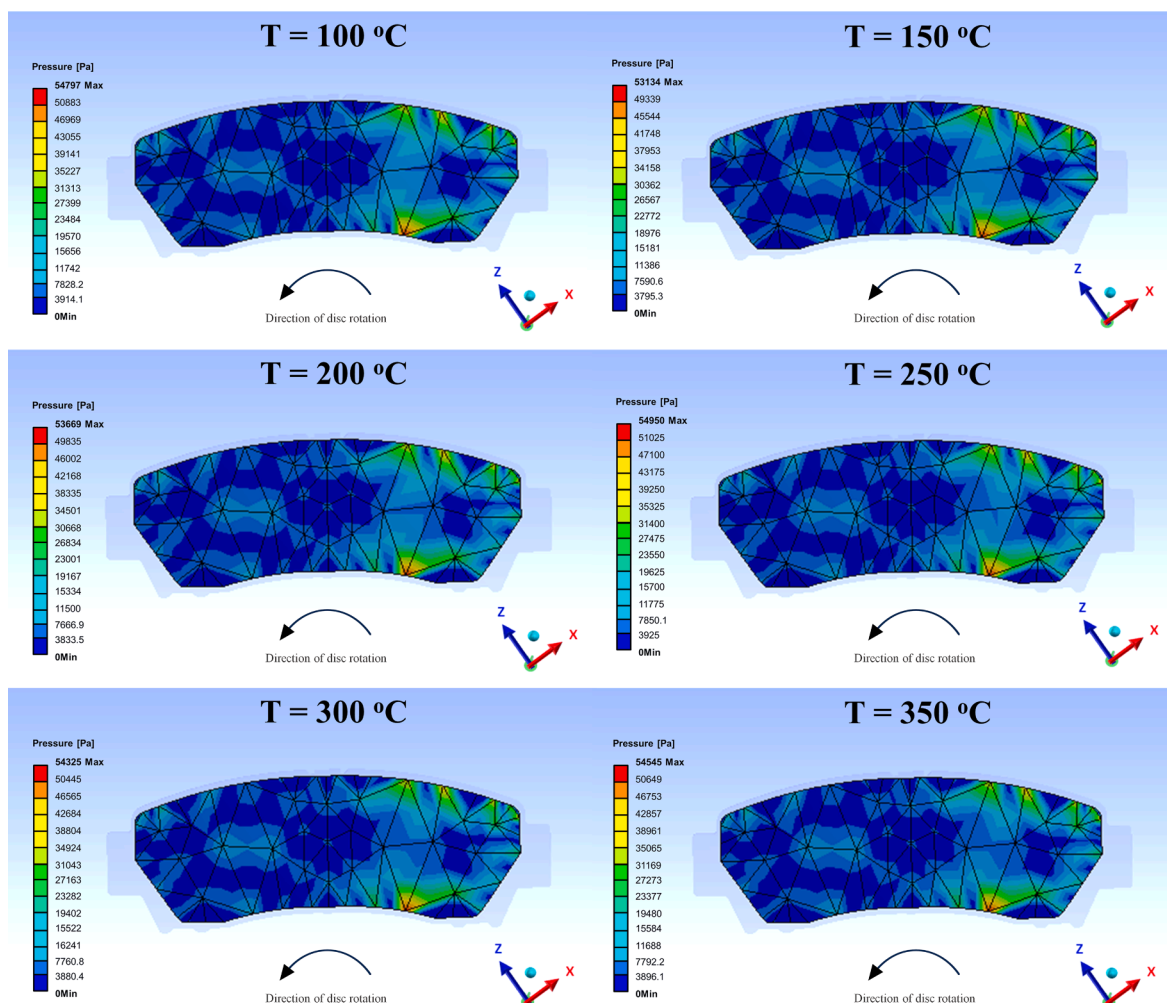


**Fig. 11.** Interface contact pressure distributions on SG/CHH (10/0)-filled poly(BA-35x) friction pad at 100 °C-350 °C.

can be seen that the addition of the CHH to substitute the SG friction modifier was found to decrease the maximum contact pressure of the poly(BA-35x) friction pad. It is possible that the higher in the COF of the SG/CHH (2/8)-filled poly(BA-35x) friction pad is accompanied by a decrease in contact pressures of the friction pad (Belhocine and Omar, 2016).

In the case of specific wear rate ( $V$ ) of the SG/CHH-filled poly(BA-35x) friction pads as also listed in Table 5 and Table 6, it was found as expected from simulation that the  $V$  of the SG/CHH (2/8)-filled poly(BA-35x) friction pad showed lower than that of the SG/CHH (10/0)-filled poly(BA-35x) friction pad. This behavior was related to their maximum contact pressures. The friction pad that showed lower maximum contact pressure would be worn harder than the friction pad having higher maximum contact pressure. In addition, the  $V$  from the wear simulation compared with that from the experimental of the poly(BA-35x) composite samples was in reasonable agreement as the difference  $V$ , i.e., lower than 3 % is within acceptable tolerance (Kim et al., 2005; Suresh et al., 2017).

#### 4. Conclusions

Eco-friendly friction composite materials from polybenzoxazine composite filled with synthetic graphite (SG) and carbonized hemp hurd (CHH) with excellent tribological, mechanical and thermal property were successfully developed. The SG/CHH-filled polybenzoxazine composite showed higher coefficient of friction, wear resistance, strength and modulus, and glass transition temperature than that of the SG-filled polybenzoxazine composite. This suggests that good interfacial adhesion between CHH and polybenzoxazine resulted in of the SG/CHH-filled polybenzoxazine composites with enhanced properties. The SG/CHH-filled polybenzoxazine composite with 2 wt% of SG and 8 wt% of CHH possessed excellent properties including flexural strength of 50.80 MPa, flexural modulus of 8.4 GPa, glass transition temperature of 225 °C, thermal degradation temperature of 409 °C, coefficient of friction of 0.40–0.43 and specific wear rate of  $0.130 \times 10^{-7}$ – $0.227 \times 10^{-7}$  in a temperature range of 100 °C–350 °C. The prediction of specific wear rate of the SG/CHH-filled polybenzoxazine composites was evaluated from contact pressure, and from finite element simulation values which are an input into Archard's wear equation. Based on the findings in this work, it can clearly be stated that simulation results and experimental results had a great agreement. Specific wear rate predictions produced by finite element simulation of the composite pad also agreed to within 97 % with the experimental measurements. This is evident that carbonized hemp hurd can be used as a sustainable friction modifier for brake pad application.

This work was supported by the Fundamental Fund 2021, Thailand Science Research and Innovation (TSRI) via Srinakharinwirot University [grant number 032/2564]; and the National Research Council of Thailand (NRCT) and Chulalongkorn University [grant number N42A660910].

#### CRedit authorship contribution statement

**Nuttarika Kumaroop:** Methodology. **Sarawut Rimdusit:** Funding acquisition, Supervision. **Phattarin Mora:** Methodology, Visualization, Writing – original draft. **Salim Hiziroglu:** Writing – review & editing. **Chanchira Jubsilp:** Conceptualization, Funding acquisition, Supervision, Writing – review & editing.

#### References

Ahmadijokani, F., Shojaei, A., Arjmand, M., Alaei, Y., Yan, N., 2019. Effect of short carbon fiber on thermal, mechanical and tribological behavior of phenolic-based brake friction materials. *Compos. B Eng.* 168, 98–105. <https://doi.org/10.1016/j.compositesb.2018.12.038>.

- Akincioglu, G., Akincioglu, S., Öktem, H., Uygur, İ., 2021a. Experimental investigation on the friction characteristics of hazelnut powder reinforced brake pad. *Rep. Mech. Eng.* 2, 23–30. <https://doi.org/10.31181/rme200102023a>.
- Akincioglu, G., Uygur, İ., Akincioglu, S., Öktem, H., 2021b. Friction-wear performance in environmentally friendly brake composites: a comparison of two different test methods. *Polym. Compos.* 42, 4461–4477. <https://doi.org/10.1002/pc.26162>.
- Aranganathan, N., Bijwe, J., 2015. Special grade of graphite in NAO friction materials for possible replacement of copper. *Wear* 330–331, 515–523. <https://doi.org/10.1016/j.wear.2014.12.037>.
- Bashir, M., Qayoum, A., Saleem, S.S., 2021. Experimental investigation of thermal and tribological characteristics of brake pad developed from eco-friendly materials. *J. Bio. Tribo. Corros.* 7, 66. <https://doi.org/10.1007/s40735-021-00502-x>.
- Belhocine, A., Omar, W.Z.W., 2016. Three-dimensional finite element modeling and analysis of the mechanical behavior of dry contact slipping between the disc and the brake pads. *Inter. J. Adv. Manuf. Technol.* 88, 1035–1051. <https://doi.org/10.1007/s00170-016-8822-y>.
- Chan, D., Stachowiak, G.W., 2004. Review of automotive brake friction materials. *Proc. Inst. Mech. Eng. d: J. Automob. Eng.* 218, 953–966. <https://doi.org/10.1243/0954407041856773>.
- Ghosh, N.N., Kiskan, B., Yagci, Y., 2007. Polybenzoxazines-new high performance thermosetting resins: synthesis and properties. *Prog. Polym. Sci.* 32, 1344–1391. <https://doi.org/10.1016/j.progpolymsci.2007.07.002>.
- Guo, L., Sato, H., Hashimoto, T., Ozaki, Y., 2010. FTIR study on hydrogen-bonding Interactions in biodegradable Polymer blends of Poly(3-hydroxybutyrate) and Poly(4-vinylphenol). *Macromolecules* 43, 3897–3902. <https://doi.org/10.1021/ma100307m>.
- He, Z., Liu, S., Zhao, W., Yin, M., Jiang, M., Bi, D., 2022. Comparative assessment of proportions of urea in blend for nitrogen-rich pyrolysis: characteristics and distribution of bio-oil and biochar. *ACS Omega.* 8, 1232–1239. <https://doi.org/10.1021/acsomega.2c06643>.
- Hwang, H., Jung, S., Cho, K., Kim, Y., Jang, H., 2010. Tribological performance of brake friction materials containing carbon nanotubes. *Wear* 268, 519–525. <https://doi.org/10.1016/j.wear.2009.09.003>.
- Ige, O.E., Inambao, F.L., Adewumi, G.A., 2019. Biomass-based composites for brake pads: a review. *Inter. J. Mech. Eng. Technol.* 10, 920–943. <https://ssrn.com/abstract=3452484>.
- Ishida, H., 1996. Process for preparation of benzoxazine compounds in solventless systems. *US* 5543516.
- Jubsilp, C., Jantaramaha, J., Mora, P., Rimdusit, S., 2021. Tribological performance and thermal stability of nanorubber-modified polybenzoxazine composites for non-asbestos friction materials. *Polymers* 13, 2435. <https://doi.org/10.3390/polym13152435>.
- Jubsilp, C., Rimdusit, S., 2017. Polybenzoxazine-based self-lubricating and friction materials. In: Ishida, H., Froimowicz, P. (Eds.), *Advanced and Emerging Polybenzoxazine Science and Technology*. Elsevier, Amsterdam, pp. 945–974.
- Jubsilp, C., Rimdusit, S., Takeichi, T., 2018. Thermal stability and thermo-mechanical properties of nanoalumina-filled poly(benzoxazine-ester) composite films. *Chem. Eng. Transac.* 70, 439–444. <https://doi.org/10.3303/CET1870074>.
- Jubsilp, C., Singto, J., Yamo, W., Rimdusit, S., 2017. Effect of graphite particle size on tribological and mechanical properties of polybenzoxazine composites. *Chem. Eng. Transac.* 57, 1351–1356. <https://doi.org/10.3303/CET1757226>.
- Kim, N.H., Won, D., Burris, D., Holtkamp, B., Gessel, G.R., Swanson, P., Sawyer, W.G., 2005. Finite element analysis and experiments of metal/metal wear in oscillatory contacts. *Wear* 258, 1787–1793. <https://doi.org/10.1016/j.wear.2004.12.014>.
- Kolluri, D.K., Ghosh, A.K., Bijwe, J., 2010. Performance evaluation of composite friction materials: influence of nature and particle size of graphite. *J. Reinf. Plast Compos.* 29, 2842–2854. <https://doi.org/10.1177/0731684410363180>.
- Kurihara, S., Idei, H., Aoyagi, Y., Kuroe, M., 2012. Binder resin for friction material, binder resin composition for friction material, composite material for friction material containing the same, friction material and production method thereof. *US* 8227390, B2.
- Lertwassana, W., Parnklang, T., Mora, P., Jubsilp, C., Rimdusit, S., 2019. High performance aramid pulp/carbon fiber-reinforced polybenzoxazine composites as friction materials. *Compos. B Eng.* 177, 107280. <https://doi.org/10.1016/j.compositesb.2019.107280>.
- Lin, H.Y., Cheng, H.Z., Lee, K.J., Wang, C.F., Liu, Y.C., Wang, W.Y., 2020. Effect of carbonaceous components on tribological properties of copper-free NAO friction material. *Materials* 13, 1163.
- Liu, X., Yu, W., 2006. Evaluating the thermal stability of high performance fibers by TGA. *J. Appl. Polym. Sci.* 99, 937–944.
- Marrot, L., Candelieri, K., Valette, J., Lanvin, C., Horvat, B., Legan, L., DeVallance, D.B., 2022. Valorization of hemp stalk waste through thermochemical conversion for energy and electrical applications. *Waste Biomass Valor.* 13, 2267–2285. <https://doi.org/10.1007/s12649-021-01640-6>.
- Mathur, R.B., Thiagarajan, P., Dhama, T.L., 2004. Controlling the hardness and tribological behaviour of non-asbestos brake lining materials for automobiles. *Carbon Lett.* 5, 6–11.
- Matykiewicz, D., 2020. Biochar as an effective filler of carbon fiber reinforced bio-epoxy composites. *Processes* 8, 724. <https://doi.org/10.3390/pr8060724>.
- Öktem, H., Akincioglu, S., Uygur, İ., Akincioglu, G., 2021. A novel study of hybrid brake pad composites: new formulation, tribological behaviour and characterisation of microstructure. *Plast. Rubber Compos.* 50, 249–261. [10.1080/14658011.2021.1898881](https://doi.org/10.1080/14658011.2021.1898881).
- Omrani, E., Menezes, P.L., Rohatgi, P.K., 2016. State of the art on tribological behavior of polymer matrix composites reinforced with natural fibers in the green materials

- world. Eng. Sci. Technol. Int. J. 19, 717–736. <https://doi.org/10.1016/j.jestch.2015.10.007>.
- Pödra, P., Andersson, S., 1999. Simulating sliding wear with finite element method. Tribol. Int. 32, 71–81. [https://doi.org/10.1016/S0301-679X\(99\)00012-2](https://doi.org/10.1016/S0301-679X(99)00012-2).
- Rimdusit, S., Kampangsaree, N., Tanthapanichkoon, W., Takeichi, T., Suppakarn, N., 2007. Development of wood-substituted composites from highly filled polybenzoxazine–phenolic novolac alloys. Polym. Eng. Sci. 47, 140–149. <https://doi.org/10.1002/pen.20683>.
- Rimdusit, S., Tanthapanichakoon, W., Jubsilp, C., 2006. High performance wood composites from highly filled polybenzoxazine. J. Appl. Polym. Sci. 99, 1240–1253. <https://doi.org/10.1002/app.22607>.
- Sahoo, S.S., Vijay, V.K., Chandra, R., Kumar, H., 2021. Production and characterization of biochar produced from slow pyrolysis of pigeon pea stalk and bamboo. Clean. Eng. Technol. 3, 100101 <https://doi.org/10.1016/j.clet.2021.100101>.
- Satapathy, B.K., Bijwe, J., 2004. Performance of friction materials based on variation in nature of organic fibres Part I. Fade and Recovery Behaviour. Wear 257, 573–584. <https://doi.org/10.1016/j.wear.2004.03.003>.
- Singh, T., 2021. Utilization of cement bypass dust in the development of sustainable automotive brake friction composite materials. Arab. J. Chem. 14, 03324. <https://doi.org/10.1016/j.arabjc.2021.103324>.
- Söderberg, A., Andersson, S., 2009. Simulation of wear and contact pressure distribution at the pad-to-rotor interface in a disc brake using general purpose finite element analysis software. Wear 267, 2243–2251. <https://doi.org/10.1016/j.wear.2009.09.004>.
- Srinivasan, P., Sarmah, K.A., Smernik, R., Das, O., Farid, M., Gao, W., 2015. A feasibility study of agricultural and sewage biomass as biochar, bioenergy and biocomposite feedstock: production, characterization and potential applications. Sci. Total Environ. 512–513, 495–505. <https://doi.org/10.1016/j.scitotenv.2015.01.068>.
- Straffelini, G., Ciudin, R., Ciotti, A., Gialanella, S., 2015. Present knowledge and perspectives on the role of copper in brake materials and related environmental issues: a critical assessment. Environ. Pollut. 207, 211–219. <https://doi.org/10.1016/j.envpol.2015.09.024>.
- Suresh, R., Kumar, M.P., Basavarajappa, S., Kiran, T.S., Yeole, M., Katara, N., 2017. Numerical simulation and experimental study of wear depth and contact pressure distribution of aluminum MMC pin on disc tribometer. Mater. Today Proc. 4, 11218–11228. <https://doi.org/10.1016/j.matpr.2017.09.043>.
- Sutikno, M., Marwoto, P., Rustad, S., 2010. The mechanical properties of carbonized coconut char powder-based friction materials. Carbon 48, 3616–3620. <https://doi.org/10.1016/j.carbon.2010.06.015>.
- Talegaonkar, R.P., Gopinath, K., 2009. Influence of alumina fiber content on properties of non-asbestos organic brake friction material. J. Reinf. Plast Compos. 28, 2069–2081. <https://doi.org/10.1177/0731684408091>.
- Umerah, C.O., Kodali, D., Head, S., Jeelani, S., Rangari, V.K., 2020. Synthesis of carbon from waste coconutshell and their application as filler in bioplast polymer filaments for 3D printing. Compos. B Eng. 202, 108428 <https://doi.org/10.1016/j.compositesb.2020.108428>.
- Wongpayakytin, A., Jubsilp, C., Tiptipakorn, S., Mora, P., Bielawski, C.W., Rimdusit, S., 2021. Effects of alkyl-substituted polybenzoxazines on tribological properties of non-asbestos composite friction materials. Polymers 13, 567. <https://doi.org/10.3390/polym13040567>.
- Wu, Y., Zeng, M., Xu, Q., Hou, S., Jin, H., Fan, L., 2012. Effects of glass-to-rubber transition of thermosetting resin matrix on the friction and wear properties of friction materials. Tribol. Int. 54, 51–57. <https://doi.org/10.1016/j.triboint.2012.05.018>.
- Xinyu, B., Cheung, L., Jieliang, K., Wei, Y., 2014. Bamboo charcoal composite fiber friction material and brake pad fabricated therefrom, and method for preparing same. CN 102977850B.